Progress in Biomaterials (2020) 9:219–237
https://doi.org/10.1007/s40204-020-00144-1

ORIGINAL RESEARCH

Surface modification of electrospun silk/AMOX/PVA nanofibers by dielectric barrier discharge plasma: physiochemical properties, drug delivery and in-vitro biocompatibility

Namita Ojah[1] · Rajiv Borah[2] · Gazi Ameen Ahmed[1] · Manabendra Mandal[3] · Arup Jyoti Choudhury[1]

Received: 27 June 2020 / Accepted: 27 October 2020 / Published online: 18 November 2020

Abstract

The naturally obtained protein *Bombyxmori* silk is a biocompatible polymer with excellent mechanical properties and have the potential in controlled drug delivery applications. In this work, we have demonstrated dielectric barrier discharge (DBD) oxygen (O_2) plasma surface modified electrospun *Bombyxmori* silk/Amoxicillin hydrochloride trihydrate (AMOX)/polyvinyl alcohol (PVA) nanofibers for drug release applications with controlled plasma treatment duration (1–10 min). The findings indicate that plasma treated electrospun nanofibers for 1–3 min exhibited significant enhancement in tensile strength, Young's modulus, wettability and surface energy. The plasma treated electrospun nanofibers for 1–5 min showed remarkable increase in AMOX released rate, whereas the electrospun nanofibers treated with plasma irradiation beyond 5 min showed only marginal increase. Moreover, the plasma treated nanofibers also exhibited good antibacterial activity against both *E. coli* (gram negative) and *S. aureus* (gram positive) bacteria. The untreated and the plasma treated silk/AMOX/PVA electrospun nanofibers for 1–3 min showed enhanced viability of primary adipose derived mesenchymal stem cells (ADMSCs) growth on them and much less hemolysis activity (< 5%). The in vitro biocompatibility of various electrospun nanofibers were further corroborated by live/dead imaging and cytoskeletal architecture assessment demonstrating enhanced cell adhesion and spreading on the plasma treated nanofibers for 1–3 min. The findings of the present study suggest that the silk/AMOX/PVA electrospun nanofibers with plasma treatment (1–3 min) due to their enhanced drug release ability and biocompatibility can be used as potential wound dressing applications.

Electronic supplementary material The online version of this article (https://doi.org/10.1007/s40204-020-00144-1) contains supplementary material, which is available to authorized users.

✉ Arup Jyoti Choudhury
choudharyajc@gmail.com

[1] Laboratory for Plasma Processing of Materials, Department of Physics, Tezpur University, Tezpur, Assam 784028, India

[2] Life Sciences Division, Institute of Advanced Study in Science and Technology, Guwahati, Assam 781035, India

[3] Department of Molecular Biology and Biotechnology, Tezpur University, Tezpur, Assam 784028, India

Graphic abstract

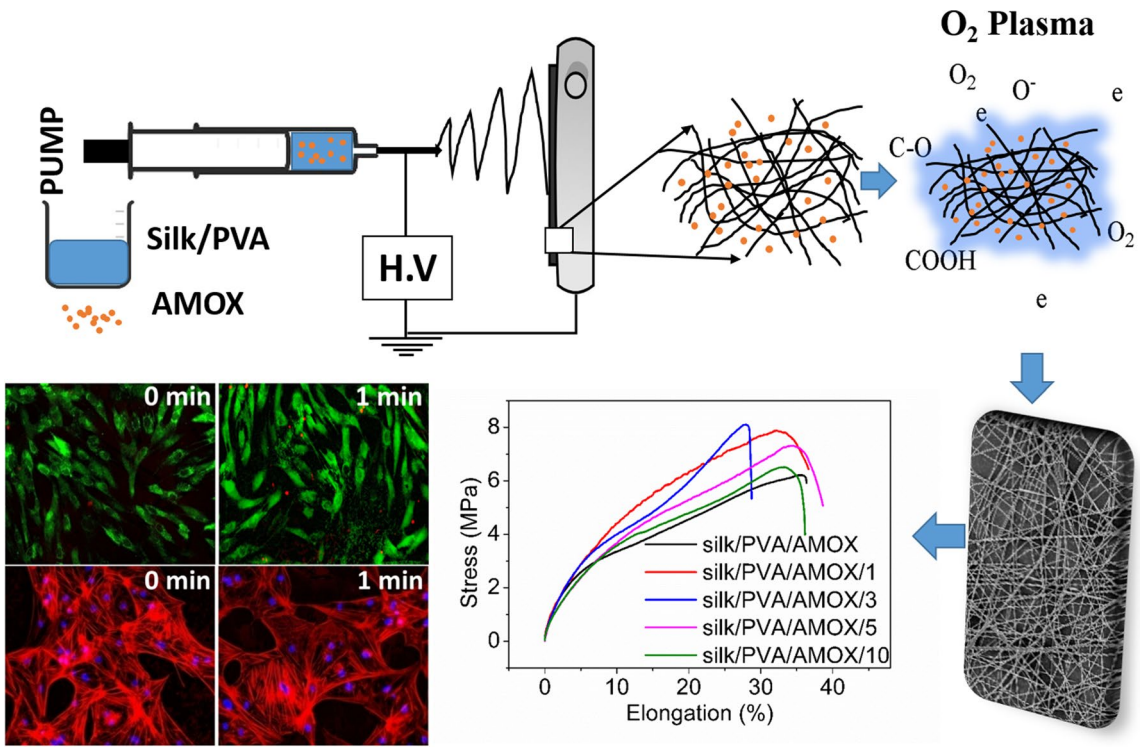

Article Highlights

- **Effect of O_2 DBD plasma treatment time on the surface properties of silk/AMOX/PVA nanofibers.**
- **Plasma treatment time of 1 min shows the highest rate of surface modifications in terms of chemical, mechanical, wettability and surface energy improvement.**
- **Increase in plasma treatment time up to 5 min results in continuous increasing drug release rate.**
- **The plasma treatment time does not cause any hemolytic effect, also improved cell viability and cell attachment with cell spreading is observed after 1–3 min of plasma treatment time.**

Keywords Silk · Dielectric barrier discharge · Surface modification · Hydrophilicity · Drug delivery · Biocompatibility

Introduction

Polymeric electrospun nanofiber-based drug delivery systems have been explored widely due to their unique porous structure and high surface to volume ratio (Shababdoust; et al. 2018; Saeed et al. 2017). The nanoscale electrospun fibers were used in therapeutic targeted drug delivery with a wide range of drug release kinetics (Ojah et al. 2019a; Kajdic et al. 2019). However, the surface properties of any material have an important role to play in specific biological applications as the surface of the material encounters the target (Nedela et al. 2017; Hetemi and Pinson 2017). It is not always likely to have all the desired properties in a single material. A few desired surface properties such as surface roughness, wettability, tensile strength etc., can be externally aided to a material using appropriate surface modification techniques (Molavi et al. 2020; Krishnakumar et al. 2019; Yoshida et al. 2013). Regarding this, the low temperature plasma surface modification of polymers have gained considerable research interest due to its energy efficient and green approach (Das et al. 2018; Ojah et al. 2019a, b). The non-uniform and highly complex plasma species (electrons, ions, neutral atoms, reactive species, metastable states etc.) transfer energy to the polymer surface through direct collision with the surface, thereby introducing new and enhanced surface properties such as surface roughness, incorporation of polar functional groups, wettability, surface energy, higher mechanical strength etc. (Das et al. 2018; Ojah et al. 2019a).

Low temperature plasma irradiation technique has been shown in the past in surface modification of polymeric

materials (Meghdadi et al. 2019; Ojah et al. 2019a, b; Theapsak et al. 2010; Chutia et al. 2019). Recently, low temperature atmospheric pressure dielectric barrier discharge (DBD) plasma has been utilized widely in various fields of material processing such as etching, surface cleaning, polymerization, surface modification, ozone generation, medical treatments and in semiconductor devices etc. (Rezaei et al. 2016; Simor et al. 2010). The plasma generation in DBD is due to the application of a very high voltage in the order of kV (Foruzan et al. 2018; Balcon et al. 2007). The DBD plasma irradiation has gained increasing popularity in materials surface engineering due to its low cost as it does not require any expensive and complicated vacuum arrangements and its simple structure (Ozkan et al. 2016; Xiaoping et al. 2012).

Plasma irradiation technique with a constant processing parameter was employed previously in surface modification of silk based biomaterials (Zhang et al. 2019; Choudhury et al. 2016; Ojah et al. 2019a, b). The versatile biopolymer silk has inspired increasing interest in the field of biomedical, pharmaceutical, optic and optoelectronic devices due to its favourable and attractive properties (Tomeh et al. 2019; Kundu et al. 2014). Silk exhibits high biocompatibility, slow degradability with mild processing conditions which makes it suitable for developing into various forms such as films, hydrogels, nanofibers and scaffolds (Kundu et al. 2014). The primary structure of silk consists of three major amino acids, namely glycine (Gly), alanine (Ala) and serine (Ser) in a ratio of 3:2:1 (Dyakonov et al. 2012). The secondary structure of silk is characterized by amorphous random coil and anti-parallel hydrogen bonded β-sheet structure (crystallizable and hydrophobic) which eventually provides good stretchability excellent mechanical strength and biocompatibility with high thermal stability (~ 250 °C) (Pollini and Paladini 2020; Yucel et al. 2014). Moreover, the presence of amino and carboxylic groups in silk fibroin aids in bio-functionalization of ligands and biomolecules for targeted drug delivery (Tomeh et al. 2019). It is also reported that silk-based drug delivery systems has the ability to enhance the stability of loaded drugs and proteins (Tomeh et al. 2019). The silk-based biomaterials undergo gel formation upon contact with aqueous media, thus diffusion of liquid into the silk matrix is followed by antibiotic particles released from the biomaterials (Dyakonov et al. 2012; Subia and Kundu 2012). Moreover, the silk fibroin has been recognized as good wound dressing biomaterial due to its ability of maintaining a moist environment at the wound site, proper air permeability and minimal inflammatory reaction. Besides, it can provide improved cell attachment and proliferation at various stages of complete wound healing process (Chouhan and Mandal 2020; Pollini and Paladini 2020; Dyakonov et al. 2012). It has also been reported that with addition of suitable antimicrobial agents, silk-based drug delivery systems have further advantages of overall improvement in mechanical properties, modification of drug release kinetics and enhanced cell adhesion with improved biocompatibility which can provide necessary supports for complete wound healing (Tomeh et al. 2019; Pollini and Paladini 2020). In the context of surface modification, it was reported that low temperature plasma can tailor the surface properties of silk-based biomaterials which eventually helps in better wettability, improved bioadhesion and higher drug loading efficiency (Ojah et al. 2019b; Ribeiro et al. 2016; Jeong et al. 2009). In addition to that, low temperature plasma has been found efficient in modulating the cell proliferation and adhesion of silk-based nanofibrous membranes (Lee et al. 2014). Moreover, plasma surface modification has also proven to be effective in improving drug release kinetics of non-degradable polymers where, plasma treatment can influence the water penetration rate of polymeric scaffolds and thereby controlling the drug release kinetics (Yoshida et al. 2013). The higher wettability of biomaterials by plasma treatment can also accelerate the degradation rate, which in turn can modify the drug release (Petlin et al. 2017). Moreover, plasma treatment is utilized to fabricate hydrophobic coatings on the material surface to delay its degradation and hence the slow drug release (Yoshida et al. 2013; Petlin et al. 2017). However, it is well established that the effect of plasma treatment on material surface depends on the processing parameters of the plasma itself and any small change in such parameters can lead to a vivid change in the surface chemistry of a material (Foruzan et al. 2018). In that regard, it is important to study the impact of varying plasma processing parameters on the material surface.

Herein, we have investigated the effect of plasma treatment by varying irradiation time on various surface properties of the electrospun *Bombyxmori* silk/Amoxicillin hydrochloride trihydrate/polyvinyl alcohol (silk/AMOX/PVA) nanofibers and showed an optimized irradiation approach to improve the drug release rate and biocompatibility of the electrospun nanofibers for potential applications in wound healing. AMOX is a well-known antibiotic effective against both gram positive and gram negative bacteria and this could be helpful in preventing bacterial growth in the wound site (Ojah et al. 2019b). To fulfill the aim, all the other operating parameters of the DBD plasma setup were kept fixed such as: the electrode gap, applying voltage and gas flow rate except the treatment time. The electrospun nanofibers were irradiated with DBD O_2 plasma by varying irradiation time for 1, 3, 5 and 10 min, while other operating parameters such as the electrode gap, applied voltage and gas flow rate of the DBD plasma setup were kept fixed. The physicochemical properties of the untreated and plasma treated electrospun nanofibers were assessed by FESEM, ATR-FTIR, tensile analyzer, and contact angle measurement analysis. Drug release behavior of different electrospun nanofibers were also studied to explore their potential in wound

healing applications. Subsequently, in-vitro biological studies were assessed with the help of hemolytic activity assay, MTS assay, live/dead and rhodamine-phalloidin staining. To evaluate the biocompatibility of various silk/AMOX/PVA electrospun nanofibers, porcine adipose derived mesenchymal stem cells (ADMSCs) were used. ADMSCs are pluripotent stem cells which can differentiate into different lineages and secrete paracrine factors for inducing tissue regeneration (Hassan et al. 2014). In fact, ADMSCs play a major role in three main phases of a wound healing process, which are inflammatory, proliferative, and remodeling phase through paracrine signalling (Demirci et al. 2018). Thus, the advances in understanding the immunosuppression and secretion of pro-angiogenic factors by ADMSCs, have inspired the scientists and researchers across the world to explore the potential of ADMSCs alone or in combination with matrix scaffold for both acute and chronic wound repairs. The goal of the present study is to fabricate and optimize a wound dressing in nanofibrous matrix form using biodegradable and biocompatible FDA approved *Bombyxmori* silk fibroin and PVA with incorporation of antibiotic AMOX, wherein dielectric barrier discharge (DBD) oxygen (O_2) plasma treatment has been employed to optimize the antibiotic release profile for infection resistance. However, we envisage that the proposed wound dressing is not limited to infection resistance but may have the potential to promote wound healing when combined with ADMSCs. Hence, the current work is also focused on preliminary evaluation of biocompatibility and cell behavior on these nanofibrous mats.

Experimental

Materials

Bombyxmori silk cocoons were collected from Central silk board, Morigaon, Assam, India. The polyvinyl alcohol (PVA) (fully hydrolyzed, M_w 145 kDa) was purchased from Merck, India. Sodium bicarbonate ($NaHCO_3$, ≥ 99%) and acetic acid (glacial, ≥ 99%) were supplied by Sigma Aldrich, India. Diiodemethane and phosphate buffer saline (PBS) were acquired from Sigma Aldrich, USA. The dialysis membrane (12 kDa molecular cut off) was supplied by Himedia, India. The antibiotic amoxicillin hydrochloride trihydrate (AMOX) and lithium bromide (LiBr) were purchased from BR Biochem Life Sciences, India and Tokyo Chemical Industries, Japan respectively. The chemicals were directly used without any further purification.

Preparation of precursor solutions and electrospinning

The *Bombyxmori* silk solution was prepared by the method already described in previous work (Ojah et al. 2019a). The final concentration of the silk solution was obtained as 6.8% (*w*/*v*). The PVA solution was prepared with a concentration of 8% (*w*/*v*) with rigorous stirring and constant heating at 80 ºC for 3 h (Das et al. 2018; Ojah et al. 2019a). The PVA and silk solutions were mixed in a ratio of 2:1 (silk: PVA) by mild stirring for 15 min. The antibiotic AMOX was added to the silk/PVA solution with concentration 1500 µg/mL with mild stirring for 15 min. The final silk/AMOX/PVA solution was then allowed to settle down prior to electrospinning. The schematic diagram and procedure of electrospinning was elaborated earlier (Das et al. 2018). Briefly, the solution was loaded into a syringe with 20 G needle and electrospun at a high voltage of 18 kV with flow rate 0.5 mL/h. The nanofibers were collected in an aluminum foil attached to a grounded static collector plate (150 mm × 150 mm). After electrospinning, the aluminum foil was collected and kept in a vacuum desiccator for future use (temperature 27 ºC, humidity 50%).

DBD plasma treatment

The experimental setup of DBD plasma treatment is reported elsewhere (Ojah et al. 2019a, b). Briefly, the setup consists of one high voltage electrode and one ground electrode (250 mm × 250 mm). Both electrodes were covered with two glass plates of thickness 3 mm. The nanofibers were peeled off from the aluminum foil prior to plasma treatment and cut into pieces of certain dimensions according to the requirement and placed at the bottom electrode of the DBD setup. The nanofibers were plasma treated at a constant applied voltage of 15 kV with an electrode gap of 6 mm. The nanofibers were plasma treated for different time periods such as 1, 3, 5 and 10 min respectively. During the experiment, continuous O_2 gas flow into the chamber with a flow rate of 2 SLPM was controlled by a mass flow controller (Alicat Scientific, India). The discharge characteristics of the DBD plasma setup was analyzed using a high voltage probe (Tetronix, P6015A, 1000:1 and a digital oscilloscope (Tetronix, TPS2024B, 200 MHz) (Ojah et al. 2019b). The discharge was found uniform throughout the whole experiment and the respective discharge current–voltage curve for these particular parameters are reported in Fig. 1. The respective electric energy (W) associated with a discharge cycle was also calculated in this work by plotting the transported charge along Y-axis and the applied voltage along X-axis which eventually gives the lissajous figure (Fig. 1) (Ray

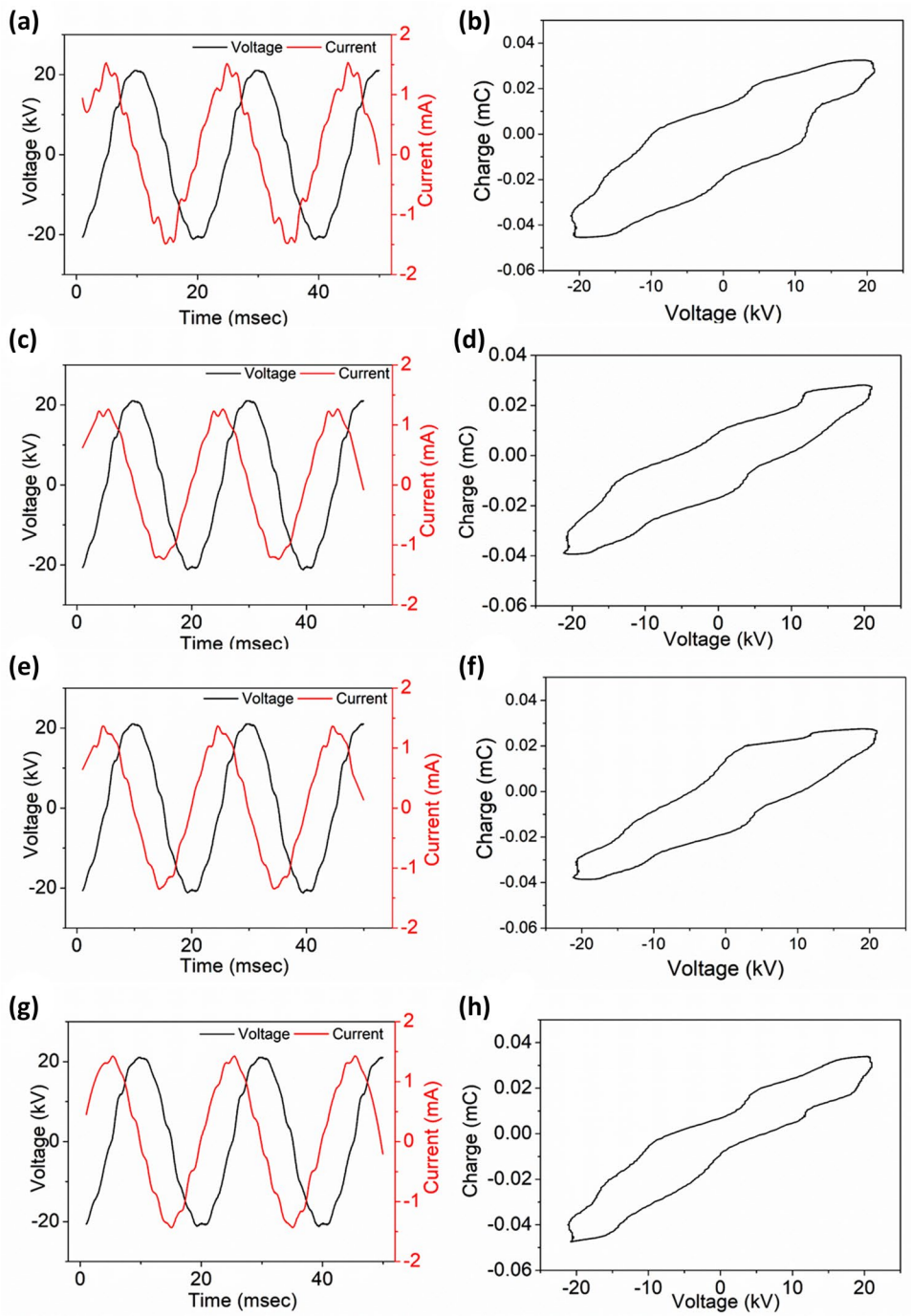

Fig. 1 Discharge characteristics of the DBD plasma at constant operating voltage of 15 kV for different treatment time. Where **a**, **b** are for 1 min; **c**, **d** are for 3 min; **e**, **f** are for 5 min and **g**, **h** are for 10 min plasma treatment time

Table 1 Discharge energy and power of the DBD plasma setup at operating voltage 15 kV, $d = 6$ mm, $f = 50$ Hz

Treatment time (min)	Discharge energy (J)	Discharge power (W)
1	0.89 ± 0.20	44.50 ± 3.28
3	0.81 ± 0.31	40.50 ± 5.32
5	0.83 ± 0.12	41.50 ± 2.95
10	0.80 ± 0.21	40.00 ± 3.14

et al. 2016; Kostov et al. 2009; Wang et al. 2012). The area enclosed by the lissajous figure automatically gives the electric energy (W) dissipated in one discharge cycle of the DBD plasma (Wang et al. 2012). However, similarly the power dissipated in one discharge cycle was also calculated in this work using the following formula and is shown in Table 1 (Ray et al. 2016; Wang et al. 2012).

$$P = f.W, \tag{1}$$

where f is the frequency of the applied voltage and W is the electric energy dissipated in one discharge cycle.

Characterization techniques

The surface morphology of the prepared silk/AMOX/PVA nanofibers were evaluated using field emission scanning electron microscope (FESEM, Zeiss, Sigma, Germany). For better comparison, the FESEM images of O_2 plasma treated nanofibers were assessed at different time intervals. For the measurement, the nanofibers along with the aluminum foil were cut into pieces of 5 mm × 5 mm and coated with gold (SC7620, Emitech) at low vacuum. The average nanofiber diameter was calculated using imageJ software.

The chemical composition analysis of the nanofibers with/without O_2 plasma treatment were evaluated by attenuated total reflectance Fourier transform infrared spectroscopy (ATR-FTIR, IMPACT 410, NICOLET, USA). The spectra were taken in transmittance mode with a spectral region of 400–4000 cm^{-1} and resolution 4 cm^{-1}.

The mechanical performances of the electrospun silk/AMOX/PVA and silk/AMOX/PVA/O_2 nanofibers were evaluated using Universal testing machine (UTM, INSTRON 4204) at a constant speed of 10 mm min^{-1} with a 10 kN load (temperature: 27 °C and humidity: 50%). The nanofibers were cut into dimensions of 10 mm × 50 mm (thickness = 0.3 mm) and a total of five measurements were made for each sample. From the stress–strain curve the tensile strength, Young's modulus and elongation-at-break (%) are calculated and reported as mean ± SD.

The wettability of the nanofibers were evaluated using water contact angle measurement employing sessile drop method (Data Physics OCA 20, Germany) (Das et al. 2018). For calculation of surface energy (γ_s) OWRK method was used, where the double distilled water and non-polar liquid diiodemethane were both dropped on the nanofiber surface and the image as well as the contact angle was recorded instantly (Das et al. 2018; Ojah et al. 2019a). The total surface energy of the silk/AMOX/PVA and silk/AMOX/PVA/O_2 nanofibers were calculated using the following relation (Das et al. 2018; Ojah et al. 2019a)

$$\gamma_s = \gamma_s^p + \gamma_s^d, \tag{2}$$

where γ_s^p and γ_s^d are polar and dispersive components of surface energy (γ_s) respectively.

To determine the surface energy (γ_s), the polar and dispersive components were calculated using the following equations using two liquids, water and diiodemethane.

$$\begin{aligned}(\gamma_s^d)^{0.5} + 1.53(\gamma_s^p)^{0.5} &= 7.80(1+\cos\theta_W)\\ (\gamma_s^d)^{0.5} + 0.22(\gamma_s^p)^{0.5} &= 3.65(1+\cos\theta_D)\end{aligned} \tag{3}$$

where θ_W and θ_D are water and diiodemethane contact angles respectively. The data was recorded at different positions of a sample of dimension 10 mm × 10 mm area.

Drug release study

The rate of AMOX release from the silk/AMOX/PVA nanofibers were evaluated by taking absorbance of PBS at 273 nm using a UV visible spectrometer (Perkin Elmer model no: Lambda 365). The untreated and O_2 plasma treated nanofibers of specific amount with three parallel sets were put into centrifuge tubes containing 10 mL PBS (pH 7.4) and were incubated at 37 °C during the whole experiment period. At certain time interval, 1 mL of PBS was taken out from the centrifuge tubes and the UV absorbance value was recorded at 273 nm immediately. To retain the final volume of the nanofiber immersed solutions, simultaneously fresh PBS solution was added into the tubes each time.

Swelling and degradation Study

The swelling study of the plasma treated and untreated silk/PVA nanofibers was carried out by their immersion into PBS (pH 7.4) at 37 °C. The initial weight (W_0) of the untreated and plasma treated electrospun nanofibers were measured carefully before their immersion into PBS. At certain time intervals the nanofibers were taken out from PBS and the excess surface water was removed by a filter paper, followed by measuring the swollen weight (W_s) of the nanofibers again and then placed in the same PBS. The swelling ratio of the nanofibers were calculated by the following equation

$$\text{Swelling ratio} = \frac{W_s - W_0}{W_0}. \tag{4}$$

The degradation test of the nanofibers before and after plasma treatment was also carried out in similar procedure. The degradation was calculated using the following formula

$$\text{Degradation}(\%) = \frac{W_0 - W_d}{W_0} \times 100, \tag{5}$$

where W_0 is the initial weight of the nanofibers before immersion into PBS and W_d is the dry weight of the nanofibers after immersion into PBS.

Water vapor transmission rate (WVTR)

The water vapor transmission rate (WVTR) was measured according to American Society for Testing and Materials (ASTM) standard (Xu et al. 2016). Briefly, the experiment was performed in a desiccator incubated at 37 °C and

relative humidity of 50%. Permeability cups were filled with 1 g of dehydrated $CaCl_2$. The cups were immediately covered with the silk/AMOX/PVA and silk/AMOX/PVA/O_2 nanofibers treated at different plasma times and sealed properly by laboratory parafilm (USA, Neenah, WI 54,956) across the edges. The weight of the whole assembly after mounting the nanofibers was measured in a digital balance (Metler, accuracy 0.0001 gm) and placed in the desiccator. An open cup was considered as control. The WVTR has been measured by calculating the weight difference of the cups after 24 h and using the following formula

$$\mathrm{WVTR} = \frac{\triangle m}{A \times \mathrm{time}}, \tag{6}$$

where $\triangle m$ is the weight difference between the cups before and after incubation and A is the surface area of the film which was exposed to air. The experiments were performed in triplicates and data are presented with mean ± SD.

Antibacterial test

The antibacterial study for all the untreated and plasma treated silk/AMOX/PVA nanofibers were evaluated for both gram positive *S. aureus* and gram negative *E. coli* bacteria. The detailed procedure for the same was reported earlier (Ojah et al. 2019a, b). Briefly, specific amount of nanofibers were placed in agar plates where bacteria was already cultured and grown fully with the help of sterilized forceps and pressed gently. The plates were incubated at 37 °C; after 24 h the plates were taken out and the images were captured by a single lens-digital reflex camera (DSLR, Nikon D7200) and reported.

In-vitro biological studies

Hemolytic activity test

For hemolysis study, fresh venous blood was used which was collected from a healthy human donor in heparinized tubes. The plasma treated/untreated silk/AMOX/PVA nanofibers (50 mm × 50 mm) were incubated with 150 µL of human blood with 10% RBC suspension (prepared by dilution with 0.9% NaCl) and volume was adjusted to 2 mL with 0.9% NaCl followed by incubation for 1 h at 37 °C. Blood incubated with 0.9% NaCl was considered as negative control and with distilled water without test material as positive control for the test. After 1 h of incubation, the reaction mixture was centrifuged at 10,000 rpm for 10 min. The free hemoglobin present in the supernatant was measured using a UV–visible spectrophotometer at 540 nm wavelength. The percentage of hemolysis was calculated using the following relation,

$$\mathrm{Hemolysis}\,(\%) = \frac{\mathrm{Abs}_{\mathrm{sample}} - \mathrm{Abs}_{-\mathrm{vecontrol}}}{\mathrm{Abs}_{+\mathrm{vecontrol}} - \mathrm{Abs}_{-\mathrm{vecontrol}}} \times 100. \tag{7}$$

Cell isolation and sample preparation

To evaluate the biocompatibility of various silk/AMOX/PVA electrospun nanofibers, porcine adipose derived mesenchymal stem cells (ADSCs) were used. ADMSCs were isolated from the subcutaneous fat as per the previously reported protocol, which was harvested from the dorsal abdominal area of porcine at a local abattoir (Williams et al. 2011). Briefly, the harvested subcutaneous fat was obtained in cold PBS. The tissue was finely minced using sterilized scissors by separating the dermal and muscle part followed by washing with cold PBS containing penicillin 100 units/mL, 100 µg/mL streptomycin and amphotericin-B 2.5 µg/mL (Gibco, USA). Then, the tissue was digested in 0.1% (*w*/*v*) Type-IA collagenase solution in incomplete DMEM (($\geq$ 125 CDU/mg, Sigma, USA) under mild shaking for 2 h at 37 °C. The digested tissue was transferred into a fresh 50 mL centrifuge tube followed by vigorous shaking for 30–60 s to promote separation of the stromal vascular fraction and neutralized by adding equal volume of DMEM with 10% (*v*/*v*) FBS. The whole mixture was centrifuged twice at 300 g for 15 min to pellet down the stromal vascular fraction. After centrifugation, the floating adipocytes were aspirated, and the cell suspension was filtered through a dual filter system into a fresh 50 mL centrifuge tube and washed twice with DMEM media. Following filtration, the cell suspension was again centrifuged at 300 g for 5 min, the supernatant aspirated, and the pelleted stromal cells resuspended in 1 mL of high glucose DMEM supplemented with 10% (*v*/*v*) FBS and 1X antibiotic/antimycotic solution. Then, the cells were plated in 90 mm Petri-dishes at a density of 6×10^5 cells/dish and incubated at 37 °C under a 5% CO_2 in air humidified atmosphere. After 24 h of initial plating, expansion medium was replaced with fresh medium to remove non-adherent cells. Thereafter, the media was changed in every 3–4 days and cells were passaged at 70–90% confluence. Cells from passages 3–5 were in further experiments.

For biological assessment, the various electrospun nanofibrous mats were cut into dimensions of 5 mm × 5 mm and sterilized by autoclaving in hydrated conditions. Prior to cell seeding, the electrospun mats were conditioned in growth media overnight and subsequently used in in vitro biological studies.

MTS cell proliferation assay

The MTS proliferation assay was carried out to evaluate the cytotoxicity of the electrospun nanofibers following

incubation with ADMSCs. Briefly, ADMSCs were seeded on different substrates at a concentration of 5×10^3 cells/well in a 96 well plate for the MTS assay. Cell viability after incubation of 24 and 48 h on the materials was quantified using Cell Titer 96® AQueous One Solution containing 3-(4,5-dimethylthiazol-2-yl)-5-(3-carboxymethoxyphenyl)-2-(4-sulfophenyl)-2*H*-tetrazolium, inner salt) (MTS). The cultured materials were washed with sterile PBS twice, and MTS reagent diluted 1:5 in media was added directly to all the wells except the blank. The plates were incubated for 2 h at 37 °C and optical density (OD) was measured at 490 nm. All experiments were performed at $n = 3$.

Live/dead staining

The viable and dead cells seeded on different electrospun nanofibers were visualized using calcein-AM and ethidium homodimer (Sigma-Aldrich) staining after 48 h of culture. Briefly, the cell seeded nanofibers were washed with PBS once and incubated at 37 °C and 5% CO_2 with 40 nM calcein-AM (stain live cells) and 20 nM ethidium homodimer (stain dead cells) for 20 min. Then, the dye was removed and washed the nanofibers twice with PBS, subsequently visualized underhydrated conditions in fluorescent microscope (EVOS XL digital microscope, Thermo Fisher Scientific, USA) with viable cells appearing green and dead cells appearing red.

Rhodamine-Hoechst staining

To visualize the cytoskeletal architecture of the cells seeded on the electrospun nanofibers, the cell seeded nanofibers were fixed with neutral buffered formalin (NBF) (Sigma-Aldrich) after 72 h of culture. The fixed constructs were treated with 0.165 µM phalloidin conjugated to rhodamine (Life technologies, USA.) to stain the F-actin and counter stained with Hoechst-33342 (Sigma-Aldrich) for nucleus. The nanofibers were then visualized under fluorescence microscope (EVOS XL Digital microscope) and representative images are presented.

Statistical analysis

The results are expressed with mean ± SD. The significant difference between various experimental sets are evaluated using one-way analysis of variance (ANOVA) followed by Tukey test for several comparisons where p value < 0.05 is considered as significant.

Results and discussion

DBD plasma characteristics

The uniform discharge mode of the DBD plasma is very much important for even surface treatment. In this work, the DBD plasma showed uniform discharge mode throughout the whole experiment and the same was confirmed from the discharge characteristics of the plasma setup. The uniform discharge current curves for different treatment times, as shown in Fig. 1, confirming the uniform discharge mode of the DBD plasma setup at operating parameters of $V = 15$ kV and $d = 6$ mm) (Ojah et al. 2019b; Wang et al. 2012). Since, the operating parameters of the DBD plasma except the treatment time were constant; therefore, the similar intensity discharge current–voltage curves are expected in each set of experiments. The lissajous figures are also plotted in Fig. 1 and the electric energy dissipated in one discharge cycle was calculated for each set of treatment time. It is expected that due to fixed plasma parameters, the energy values and the shape of the lissajous figures should remain almost similar in each time. The calculated electric energy dissipated in one discharge cycle were found to be 0.89 J, 0.81 J, 0.83 J and 0.80 J for 1, 3, 5 and 10 min of treatment time, respectively. From the electric energy, the discharge power was calculated and is depicted in Table 1. It is clear that the discharge energy remains similar for all the set of treatments due to the fixed applied voltage, frequency (50 Hz) and discharge gap. Therefore, the overall average discharge power for operating voltage 15 kV with electrode gap 6 mm was calculated as 41.62 ± 2.01 W.

Surface morphology analysis

Figure 2 shows the FESEM images of untreated and plasma treated silk/AMOX/PVA nanofibers, confirming the formation of beads free and randomly oriented nanofibers with average fiber diameter of 140 ± 5.23 nm. However, the FESEM images do not reveal any noticeable changes in the surface morphology of the nanofibers after O_2 plasma treatment independent of the treatment time. The average diameter of the plasma treated nanofibers was also evaluated for better comparison and it was found as similar (140 ± 4.35 nm) to the untreated nanofibers independent of the treatment time. In earlier work, similar results were reported with constant plasma treatment time of 1 min (Das et al. 2018; Ojah et al. 2019a). However, no morphological changes in the nanofibers structure were observed with increasing plasma treatment time in the present work.

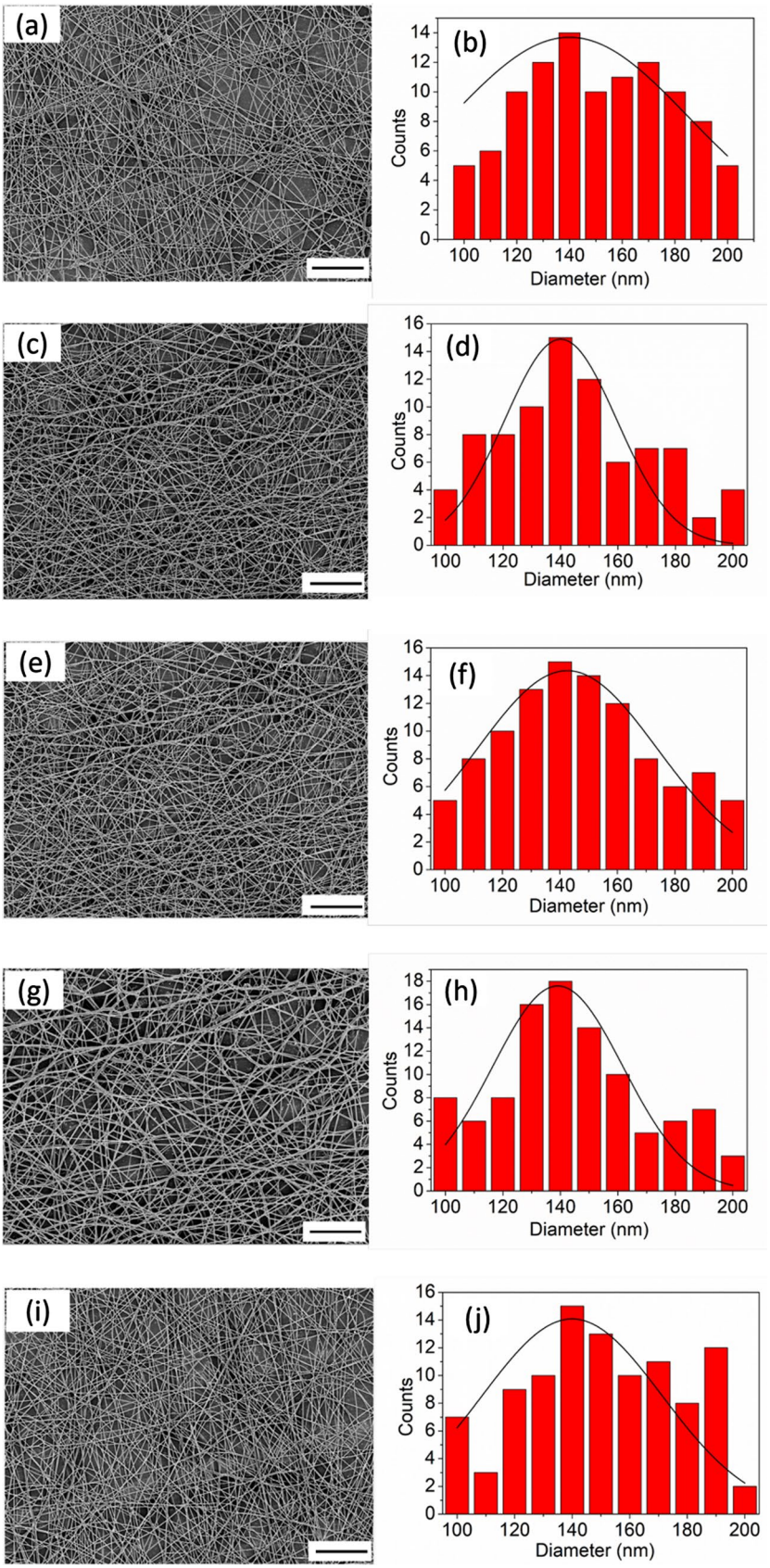

Fig. 2 FESEM images and diameter distribution of the untreated and plasma treated silk/AMOX/PVA nanofibers. Where **a**, **b** are untreated; **c**, **d** are 1 min plasma treated; **e**, **f** are 3 min plasma treated; **g**, **h** are 5 min plasma treated and **i**, **j** are 10 min plasma treated silk/AMOX/PVA nanofibers (FESEM image, scale:10 µm)

Table 2 Water contact angle and surface energy

Samples	Water contact angle (°)	Polar (mJm^{-2})	Dispersive (mJm^{-2})	Total S.E. (mJm^{-2})
Silk/AMOX/PVA	78.20 ± 2.16	2.54 ± 0.32	48.30 ± 2.35	50.84 ± 2.35
Silk/AMOX/PVA/1 min	31.50 ± 3.39	29.78 ± 1.32	37.22 ± 1.38	67.00 ± 1.90
Silk/AMOX/PVA/3 min	29.50 ± 1.80	35.45 ± 2.30	35.89 ± 1.58	71.34 ± 2.79
Silk/AMOX/PVA/5 min	27.91 ± 1.86	36.55 ± 1.20	35.65 ± 3.58	72.20 ± 3.77
Silk/AMOX/PVA/10 min	26.80 ± 3.74	36.98 ± 1.58	35.52 ± 2.85	72.50 ± 3.02

Wettability and surface energy measurements

The contact angle measurement is the simplest way to measure the wettability of any polymeric surface. Table 2 shows the water contact values for the untreated and O_2 plasma treated silk/AMOX/PVA nanofibers. The untreated nanofiber showed average water contact angle value of 78.20 ± 5.30° and the plasma treated nanofibers showed significantly lower contact angle value as compared to the untreated nanofiber. The contact angle dropped rapidly to 31.50 ± 3.39° and 27.50 ± 1.80° just after plasma treatment of 1 and 3 min, respectively, indicating improved wettability of the electrospun mats. However, with further increase in treatment time up to 5–10 min no such significant reduction of contact angle was observed.

The higher wettability generally results in higher surface energy of a polymer surface and O_2 plasma treatment improves wettability by incorporating oxygenated polar functional groups (O, O_2, O_2^-, COOH, C = Oetc.) to the surface (Das et al. 2018; Ojah et al. 2019a, b). These polar functional groups attached to the nanofibers surface strongly interacts with the water molecules resulting in lower water contact angle value (Das et al. 2018; Ojah et al. 2019a). The schematic representation of such interactions were reported elsewhere (Ojah et al. 2019a). Therefore, the respective surface energies along with their polar and dispersive components were determined to assess the surface polarity of the electrospun mats. Table 2 shows that after plasma treatment the polar components have been increased significantly as well as the surface energy also increased consequently. This improvement is a direct indication of incorporation of polar functional groups to the silk/AMOX/PVA nanofiber surface after plasma treatment (Das et al. 2018; Ojah et al. 2019a). However, after 5–10 min of plasma treatment, no further significant improvement is observed in surface energy and its polar component. It indicates that the surfaces were saturated beyond plasma treatment for 3 min.

Mechanical properties

The mechanical properties of the silk/AMOX/PVA nanofibers were evaluated in terms of its tensile strength, Young's modulus and elongation-at-break (%). For better understanding of the effect of O_2 plasma treatment, the mechanical properties of the plasma treated nanofibers for different times were also evaluated and are presented in Table 3. The untreated nanofibers exhibit tensile strength value of 6.22 ± 1.20 MPa with Young's modulus 61.29 ± 5.28 MPa. However, after O_2 plasma treatment, reasonable improvement in the tensile strength as well as in the Young's modulus values are observed. The electrospun nanofibers with plasma treated for 1 min shows improved tensile strength of 7.91 ± 1.31 MPa and Young's modulus of 67.60 ± 6.37 MPa. Similarly, the nanofibers plasma treated for 3 min shows further enhanced value of tensile strength (8.15 ± 1.26 MPa) and Young's modulus (68.22 ± 3.98 MPa). The reason behind such improvement can be explained by formation of hydrogen bonds on the nanofiber surface after O_2 plasma treatment (Das et al. 2018; Ojah et al. 2019a). As mentioned in earlier reported work, the oxygenated species formed during O_2 plasma treatment not only attaches to the nanofiber surface through hydrogen bonding but also they form hydrogen bonds among themselves (Das et al. 2018; Ojah et al. 2019a, b). This hydrogen bonded assembly leads to an extraordinarily complex structure at the nanofiber surface and eventually this contributes to the enhanced mechanical performance of the nanofibers (Das et al. 2018; Ojah et al. 2019a, b). Therefore, it is expected that number of

Table 3 Mechanical properties of the silk/AMOX/PVA nanofibers with and without plasma treatment

Sample	Tensile strength (MPa)	Young's modulus (MPa)	Elongation (%)
Silk/AMOX/PVA	6.22 ± 1.20	61.29 ± 5.28	35.72 ± 4.61
Silk/AMOX/PVA/1 min	7.91 ± 1.31	67.60 ± 6.37	32.31 ± 3.64
Silk/AMOX/PVA/3 min	8.15 ± 1.26	68.22 ± 3.98	27.82 ± 3.71
Silk/AMOX/PVA/5 min	7.33 ± 2.01	61.68 ± 6.98	34.28 ± 4.31
Silk/AMOX/PVA/10 min	6.53 ± 1.07	53.48 ± 6.87	33.12 ± 3.64

hydrogen bonds with incorporation of oxygenated plasma species should be higher with higher treatment time and due to which the 3 min plasma treated nanofiber shows better mechanical properties than 1 min plasma treated nanofibers. However, this always cannot be true as there must be a saturation point for each type of surface modification. Eventually, it was reported that after longer exposure to plasma species a surface may experience dehydration and etching which results in loosing of inherent strength of the polymer chains due to which weak mechanical properties may result (Baltazar-y-Jimenez et al. 2008). In this work, similar results are observed after 5 and 10 min of plasma treatment, where the mechanical performance of the nanofibers in terms of tensile strength and Young's modulus decrease further. Therefore, 1–3 min of DBD plasma treatment time should be sufficient for improvement of mechanical properties of silk/AMOX/PVA nanofibers. However, the rate of improvement of tensile strength from untreated to 1 min plasma-treated silk/AMOX/PVA nanofiber has been found to be much higher (27.17%) than when compared to that of 1–3 min plasma-treated nanofibers (3.03%). Therefore, it is obvious that major part of the modifications was already facilitated by 1 min O_2 plasma treatment. However, with increase in tensile strength, the elongation-at-break is found to be decreased after O_2 plasma treatment. This indicates incorporation of rigidity or stiffness to the nanofiber surface through O_2 plasma treatment (Das et al. 2018; Ojah et al. 2019a, b).

Chemical analysis

The chemical properties of the nanofibers were studied with the help of ATR-FTIR analysis. Figure 3a shows the ATR-FTIR spectra of *Bombyx mori* silk, PVA, AMOX and silk/AMOX/PVA nanofiber. The *Bombyx mori* silk shows its characteristic peaks at 1619, 1511 and 1228 cm^{-1} which corresponds to amide-I (C = O stretching), amide-II (secondary NH bending), and amide-III (C–N and N–H functionalities) respectively (Ojah et al. 2019a). The wide-ranging band between 3000 and 3500 cm^{-1} corresponds to the overlapping of hydrogen bonded -OH stretching vibration and -NH stretching vibrations of the primary amine groups (Ojah et al. 2019a). PVA shows the -OH stretching vibration of intermolecular and intramolecular hydrogen bonding at 3276 cm^{-1}, the symmetric and asymmetric vibrations of CH groups are found at 2941 and 2910 cm^{-1}, respectively (Ojah et al. 2019a). The other characteristic peaks of PVA have been observed at 1650, 1542, 1416 and 1378 cm^{-1} which

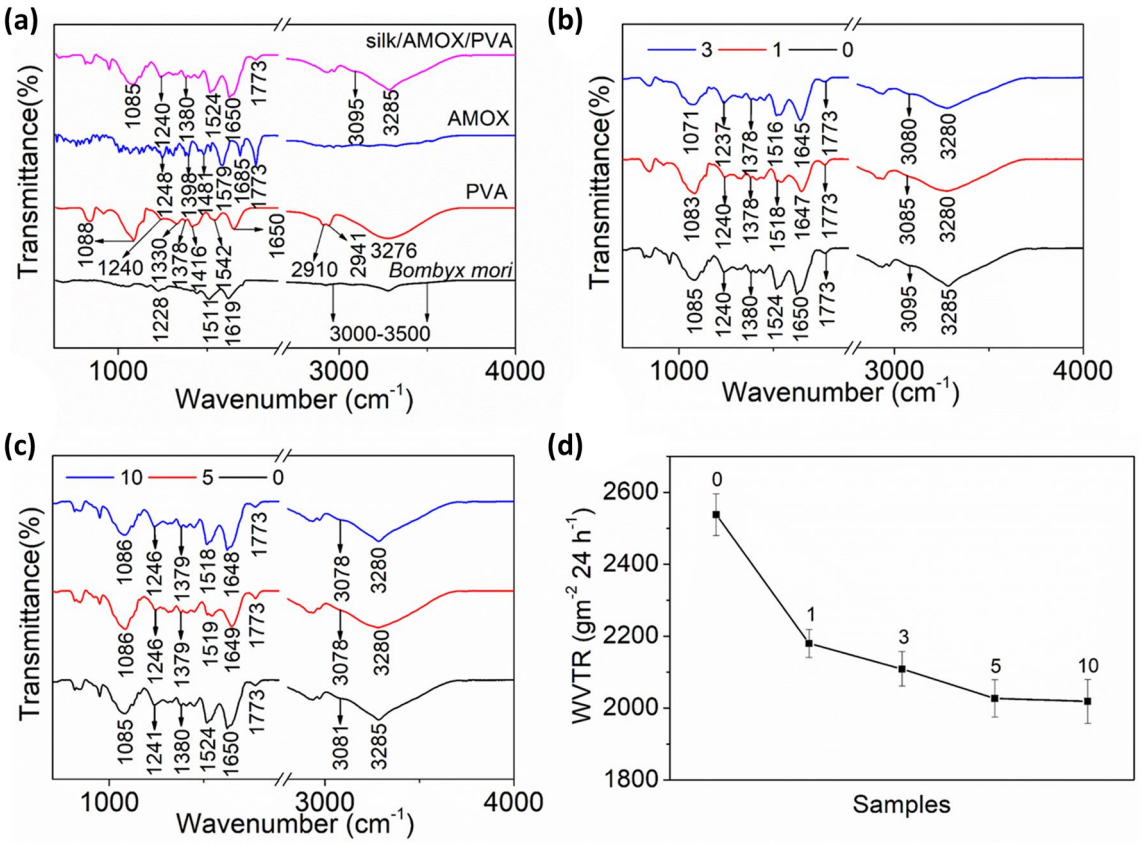

Fig. 3 **a**–**c** ATR-FTIR and **d** WVTR of the plasma treated and untreated silk/AMOX/PVA nanofibers. Where 0 indicates untreated silk/AMOX/PVA nanofibers and 1, 3, 5 and 10 indicates silk/AMOX/PVA nanofibers plasma treated for 1, 3, 5 and 10 min respectively

correspond to the C–O stretching vibrations, C = C stretching vibrations, CH_2 bending vibrations and CH stretching vibrations respectively (Das et al. 2018; Ojah et al. 2019a). The peaks at 1330, 1240 and 1088 cm^{-1} are due to CH deformation, CH wagging and C–O stretching vibrations of acetyl groups (Ojah et al. 2019a). The ATR-FTIR spectra of AMOX was also evaluated for a better comparison. The characteristic peaks of AMOX are observed at 1773, 1685, 1481 and 1248 cm^{-1} which correspond to the β-lactam ring of AMOX, C = O stretching vibration (amide I), N–H bending of secondary amine/C–C stretching of aromatic ring and C–N stretching vibration of primary amine (Ojah et al. 2019a, b). The peaks at 1579 and 1398 cm^{-1} correspond to the asymmetric and symmetric vibrations of carboxylate COO^- group (Ojah et al. 2019a, b). The ATR-FTIR curve for the composite nanofiber silk/AMOX/PVA was also plotted for further understanding. The composite nanofiber shows both peaks of silk and PVA. Furthermore, the peaks of AMOX are also clearly observed in the nanofiber backbone.

To evaluate the possible effects of O_2 plasma treatment time on the nanofiber chemical structure, the ATR-FTIR spectra of the plasma treated nanofibers at different times were also plotted for clear understanding and evaluations. All the nanofibers, independent of the treatment time, show the silk, PVA and AMOX peaks clearly. However, few changes are observed in the ATR-FTIR spectra of the plasma-treated nanofibers in terms of their peak positions.

The ATR-FTIR spectra of O_2 plasma treated silk/AMOX/PVA nanofibers are plotted in Fig. 3b, c. A one minute plasma-treated silk/AMOX/PVA nanofibers show broadening and shifting of the OH-NH band (3285–3280 cm^{-1}) towards lower wavenumber. The shifting and broadening of this band is due to incorporation of polar functional groups on the silk/AMOX/PVA nanofibers surface which is also evidenced in water contact angle and surface energy calculations (Das et al. 2018; Ojah et al. 2019a). The change in surface chemistry of the nanofibers after plasma treatment is also evidenced by shifting of the peaks 3095, 1650, 1524, 1380 and 1085 cm^{-1} simultaneously towards lower wavenumbers such as 3085, 1647, 1518, 1378 and 1083 cm^{-1} respectively. These observations are clearly proof of hydrogen bond formation as well as incorporation of oxygen species such as O, O_2, O_2^- etc., on the silk/AMOX/PVA nanofibers surface (Das et al. 2018; Ojah et al. 2019a; Baltazar-y-Jimenez et al. 2008). Similar changes are observed after increasing the plasma treatment time up to 3 min. The peaks have also shifted slightly further towards lower wavenumbers region after 3 min plasma treatment. However, after further increasing the treatment time up to 5 and 10 min, no further shifting of the peak positions are observed. The results are in accordance with other characterizations performed in this work. The incorporation of polar functional groups and increase in surface energy of the silk/AMOX/PVA nanofibers is observed to be saturated after 3 min of plasma treatment and hence similar pattern is also observed in the ATR-FTIR analysis in terms of the bands shifting after 3 min of plasma treatment time. Therefore, increasing treatment time beyond 3 min can have no further significant change in the surface chemistry of silk/AMOX/PVA nanofiber.

Water vapor transmission rate study

It was already reported that the cells in a desiccated wound may lose its vitality and functionality and as a result it can die easily (Xu et al. 2016). Furthermore, the dressing in a dehydrated wounded surface is expected to shrink easily and consequently the wound edge exposure might occur which can break the bacterial barrier (Ujang et al. 2014; Queen et al. 1987). Therefore, a good WVTR is important for specific wounds to preserve the hydration and lock moisture into the wounded skin to heal quicker (Xu et al. 2016; Queen et al. 1987). A typical of 2000–2500 gm^{-2} 24 h^{-1} has been considered as standard WVTR for convenient wound dressing, where WVTR values closer to the lower limit (~ 2000 gm^{-2} 24 h^{-1}) are found very suitable for practical applications (Queen et al. 1987). In this work, the WVTR for the silk/AMOX/PVA nanofibers was found to be 2538 ± 58 gm^{-2} 24 h^{-1} which is towards the higher side of the standard limit. Similarly, the WVTR calculated for the O_2 plasma treated nanofibers were found as 2180 ± 39 gm^{-2} 24 h^{-1}, 2109 ± 48 gm^{-2} 24 h^{-1}, 2027 ± 52 gm^{-2} 24 h^{-1} and 2019 ± 61 gm^{-2} 24 h^{-1} respectively for 1, 3, 5 and 10 min of plasma treatment, respectively. The data are plotted in Fig. 3d for the untreated and plasma-treated silk/AMOX/PVA nanofibers. It is observed that with increasing treatment time the WVTR decreases continuously up to 5 min and thereafter it becomes almost saturated. Therefore, it is observed that the plasma treatment gives a much stronger barrier for the water vapor to pass through the nanofiber area. Similar work was reported already, where low temperature plasma treatment was utilized to improve the barrier properties of polymeric films or scaffolds (Wang et al. 2011). However, in this work, the WVTR rates after plasma treatment are not only still under the standard limit but also it is much closer to the lower limit of the standard values which is to a certain extent much acceptable in case of a good wound healing scaffold (Queen et al. 1987).

Drug release study

The drug release rate of silk/AMOX/PVA nanofiber was studied until saturation was obtained in the release profile. The standardization graph and the release profiles of the untreated and O_2 plasma treated nanofibers are shown in Fig. 4. It is observed that all the nanofiber showed a faster

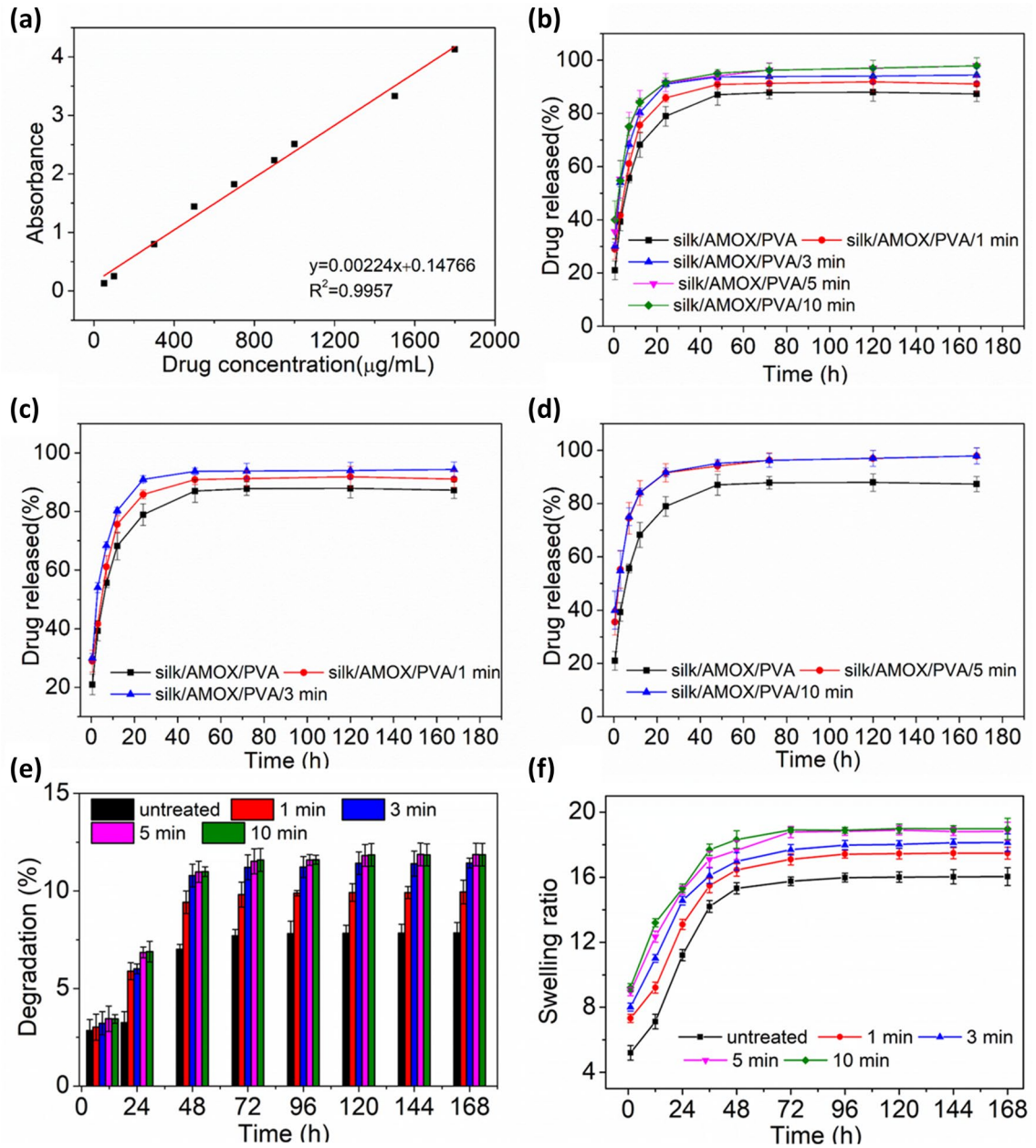

Fig. 4 **a** Standardization graph for AMOX released in PBS 7.4pH for different drug concentrations. **b–d** are drug release profiles of the plasma treated and untreated silk/AMOX/PVA nanofibers with different treatment time ranging from 1 to 10 min**. e** and **f** are degradation (%) and swelling ratio of the untreated and plasma treated silk/PVA nanofibers for 1, 3, 5, 10 min respectively

and continuous drug release rate up to 3 days and thereafter saturation was obtained. The untreated nanofiber showed a release of 78.94% after 24 h. At the same time the plasma treated nanofibers showed a release of 85.83%, 90.97%, 91.55% and 91.71% respectively after 1, 3, 5 and 10 min of plasma treatment. Therefore, most of the drug release was observed within just 24 h of incubation time. Moreover, a comparatively higher drug release rate was observed after plasma treatment. The drug release rate was found to be higher with increase in treatment time up to 5 min and thereafter no further increase in drug release rate was observed, even for increasing treatment time up to 10 min. The increase in drug release rate with plasma treatment is due to increase in wettability of the nanofibers after plasma treatment (Ojah et al. 2019a). As observed from the water contact angle measurement, the wettability was increased with increasing treatment time and it saturates after 3–5 min of treatment time. Therefore, it is expected that the nanofiber with higher wettability would tend to degrade faster (Ojah et al. 2019a). The degradation of the nanofibers is presented

in Fig. 4e. From Fig. 4e, a low percentage of degradation was observed which is due to the PVA content of the nanofibers as the *bombyx mori* silk has a slow degradation rate in neutral PBS (Liu et al. 2015). The increase in percentage of degradation will result in release of more encapsulated AMOX particles from the nanofiber backbone (Ojah et al. 2019a) and, therefore, increase in drug release rate was recorded for plasma treated electrospun nanofibers. However, in the drug release process from the nanofibers, along with degradation the swelling also plays an important role (Ojah et al 2019b). The β-sheet structure of the silk fibroin gives rise to its characteristic hydrophobicity, crystallinity and insolubility in neutral aqueous medium (Tomeh et al. 2019; Kundu et al. 2014). The silk fibroin begins to swell and form gel-like consistency as soon as it encounters the aqueous medium (Dyakonov et al. 2012; Pollini and Paladini 2020). The gel transition causes hydration and relaxation of the silk polymer chains (Dyakonov et al. 2012; Subia and Kundu 2012). This would cause the drug molecules being lost from the nanofiber backbone and releasing of the drug into the aqueous medium is observed. Therefore, this could also be a reason behind the release of AMOX particles attached onto the nanofibers (Subia and Kundu 2012; Ojah et al 2019a, b). The swelling ratio of the nanofibers is reported in Fig. 4f. It is observed that the plasma treatment enhances the swelling ratio of the nanofibers, which increases with increasing treatment time and eventually saturates after 5 min of treatment time.

However, the drug release rate observed in this case is found much higher than earlier reported work (Ojah et al. 2019a). The silk/PVA nanofiber reported earlier showed a comparatively slower drug release rate for a longer period of time due to its core–shell structure (Ojah et al. 2019a). The drug was enclosed by PVA barrier, and therefore, it took longer to be released from the nanofiber structure (Ojah et al. 2019a). However, in case of silk/AMOX/PVA nanofiber, the antibiotic drug AMOX has been encapsulated at the surface as well as within the nanofibers porous structure. Therefore, it is obvious to observe faster drug release rates in this case. The drugs present at the surface will release as soon as it comes into contact with the aqueous media and the rest will eventually release with increase in incubation time through degradation and swelling as discussed above.

Antibacterial activity

Figure 5 shows the antibacterial test results against *E. coli* (gram negative) and *S. aureus* (gram positive) bacteria for the untreated and plasma-treated silk/AMOX/PVA nanofibers after 24 h of incubation. All the nanofibers showed almost clear inhibition zone against both bacteria. The untreated silk/AMOX/PVA nanofibers showed minimal inhibition zone of 21.45 ± 4.36 mm and 31.87 ± 5.36 mm against *E. coli* and *S. aureus*. The respective zone of inhibition for all the nanofibers against both *E. coli* and *S. aureus* is represented in Fig. 5. The inhibition zone for the untreated nanofibers starts to decrease from the next day and finally vanishes after 72 h. However, plasma-treated nanofibers with variable time showed a slightly higher inhibition zone compared with untreated nanofibers. The plasma-treated nanofibers with longer treatment time showed increasingly higher inhibition zone. The higher drug release after plasma treatment is the reason behind such greater inhibition zone. All the other plasma-treated nanofibers (1, 3, 5 min) showed clear inhibition zone for 48 h, which later decreased gradually and finally vanished after 120 h.

Hemolytic activity analysis

To explore the potential application of the electrospun nanofibers as a wound dressing, hemocompatibility of all the nanofibers was assessed with the help of hemolysis activity assay. The hemolysis activity of various O_2 plasma-treated and untreated electrospun silk/AMOX/PVA nanofibers is shown in Fig. 6a. All the electrospun nanofibers show much less hemolysis activity below 0.4%, suggesting their hemocompatibility behavior, when compared to the positive control in 100% cell lysis. However, there is no statistical difference in the percentage of hemolysis activity among the O_2 plasma-treated and untreated nanofibers. The percentage of hemolysis activity of the untreated nanofibers and O_2 plasma-treated nanofibers for 1 and 3 min are almost similar, whereas nanofibers treated with O_2 plasma for 5 and 10 min are slightly higher (Fig. 6a). The slight variations in this observation have been discussed below.

The intrinsic hemocompatibility of silk fibroin and PVA is already demonstrated (Marilia et al. 2014; Nuno et al. 2014). O_2 gas plasma is very reactive etching agent due to higher electronegativity of oxygen. The successful incorporation of oxygen containing polar functional groups (viz. hydroxyl (-OH), aldehyde (-CHO), carboxyl (-COOH), etc.) after O_2 plasma treatment was demonstrated by ATR-FTIR results. It is likely possible that the increased surface hydrophilicity (as indicated by contact angle measurement and analysis) due to incorporation of the above polar functionaries, aid the covalent interaction between the nanofibers and the cell surface proteins leading to minimal hemolysis. Additionally, O_2 plasma treatment also creates intermediate free radicals on polymer surface as previously reported (Kumar and Borah 2016). Hence, the possible minute concentration of the free radicals created due to longer O_2 plasma treatment (5 and 10 min) may evoke electrostatic interaction

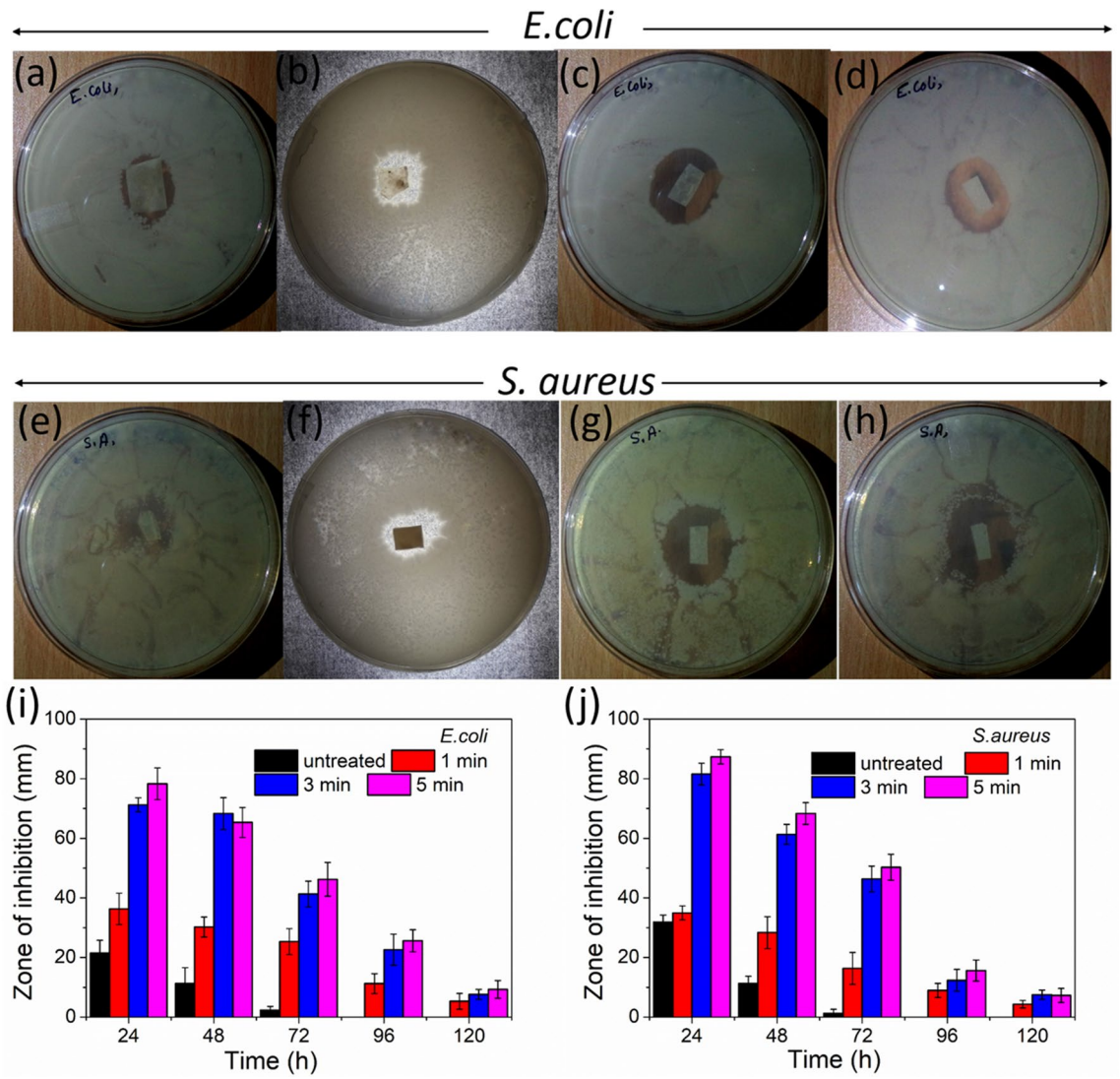

Fig. 5 Antibacterial activities of the untreated and plasma treated nanofibers against *S. aureus* and *E. coli* bacteria. Where, **a**, **e** are untreated; **b**, **f** are 1 min; **c**, **g** are 3 min; **d**, **h** are 5 min plasma treated nanofibers. **i** and **j** are zone of inhibition for the untreated and plasma treated silk/AMOX/PVA nanofibers for 1, 3, 5 min respectivelyagainst *E. coli* and *S. aureus* bacteria

between the nanofiber surface and cell surface, leading to slight increase in the hemolysis percentage.

Overall, the results suggest that there is no adverse effect of O_2 plasma treatment on the electrospun nanofibers, which causes very less hemolysis (below 0.4%) well within the acceptable limit of 5% hemolysis to qualify for biological applications.

Cell viability test

In vitro cell viability studies were carried out to investigate the cytocompatibility of the various electrospun nanofibers by MTS proliferation assay and live/dead staining of primary ADMSCs. The MTS results are presented in terms of percentage cell viability after 24 and 48 h of culture time on various electrospun nanofibers, as shown in Fig. 6b. The results reveal that all the nanofibers (both O_2 plasma-treated and untreated) supported cell growth viability of 70–80% at the initial 24 h except the nanofibers treated with O_2 plasma for 1 min revealing slightly higher 80% cell viability, which is an accepted value for biocompatible materials (Bae et al. 2012). However, after 48 h, all the electrospun nanofibers supported more than 80% cell viability, with O_2 plasma-treated nanofibers for 1 and 3 min showing more than 100% cell viability. Biocompatibility of the silk fibroin and PVA is well explored which supports the observed cytocompatibility of the untreated nanofibers (Wang et al. 2006; Gomide et al. 2012). The MTS results are in well agreement with the

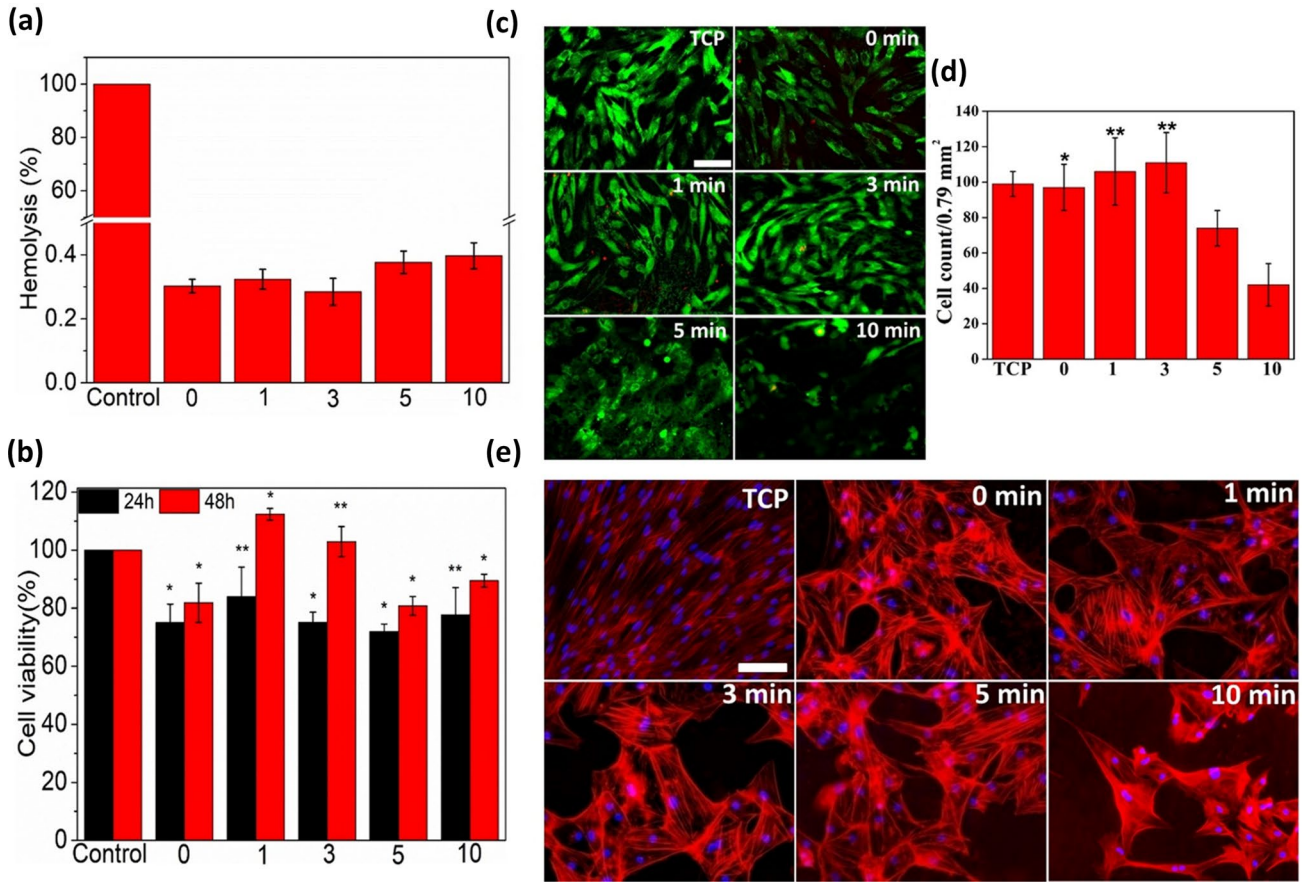

Fig. 6 In-vitro biological studies results. **a** Percentage of hemolysis (Mean ± S.D, $n = 3$) shown by untreated and O_2 plasma treated silk/AMOX/PVA nanofibers, where, 0 indicates untreated nanofibers and 1, 3, 5 and 10 indicates plasma treated nanofibers for 1, 3, 5 and 10 min, respectively, as compared to positive control (Triton X 100). **b** Percentage cell viability on different silk/AMOX/PVA nanofibers as compared to tissue culture plastic (TCP) as a negative control. **c** Representative fluorescent images of ADMSCs stained with calcein AM (green) and EthD-1 (red) during live/dead assay after 48 h of culture on control TCP and the different electrospun nanofibers as indicated. **d** Live cell count on untreated and plasma treated electrospun nanofibers. **e** Representative fluorescent images of ADMSCs stained with rhodamine phalloidin for the actin filaments (red) and nuclei counterstained with Hoechst (blue) after 72 h of culture on control TCP and different electrospun nanofibers as indicated. *and **indicate statistically significance at $p < 0.05$ and $p < 0.01$. [Microscope image, scale: 200 mm]

hemolysis activity results in the sense that the silk/AMOX/PVA electrospun nanofibers treated with O_2 plasma for 1 and 3 min demonstrated the higher cell growth and hemocompatibility, when compared to those of the untreated and the other plasma-treated nanofibers for longer period. In fact, all the O_2 plasma-treated silk/AMOX/PVA electrospun nanofibers supported significantly higher cell growth when compared to that of the untreated nanofibers. This can be attributed to the incorporation of oxygen-containing polar functionalities on the nanofiber's surface leading to favorable cell-biomaterial interaction for cell growth. This initial observation suggests no cytotoxic effect of the O_2 plasma treatment on cell growth. Yet the plasma-treated nanofibers for 1 and 3 min demonstrated highest viability of the primary mesenchymal stem cells even more that on the control tissue culture plastic (TCP), which are statistically significant.

To further confirm the MTS results, the live/dead assay was performed to visualize the viable ADMSCs cultured on different electrospun nanofibers by staining the cells with calcein AM (stained live cells in green) and EthD-1 (stained dead cells in red) after 48 h of culture. Representative fluorescent images of the ADMSCs seeded on the untreated and O_2 plasma- treated silk/AMOX/PVA nanofibers are shown in Fig. 6c. The green-fluorescent calcein AM can be visualized throughout almost all the cell bodies seeded on different electrospun nanofibers indicating the viable cells, except few dead cells (red). For further validation, live cell counting has been performed using calcein AM stained (green) cells and is presented in Fig. 6d. It has been observed that O_2 plasma-treated electrospun nanofibers for 1 and 3 min showed significantly higher live cell density, i.e., 107 ± 19/per image and

111 ± 16/per image, respectively than that on the untreated (95 ± 13/per image) and other O_2 plasma-treated electrospun nanofibers for 5 min (74 ± 12/per image) and 10 min (42 ± 10/per image) ($p \leq 0.01$) and the untreated (95 ± 13/per image) nanofibers ($p \leq 0.05$). However, there are no statistical differences in live cell density exist between the control TCP and the 1 and 3 min plasma treated nanofibers. This indicates that 1 and 3 min plasma treated nanofibers exhibit similar live cell density to that on the control TCP indicating good cell viability and adhesion, while other plasma treated nanofibers for 5 and 10 min revealed significantly less live cell density indicating poor cell viability and adhesion. The ADMSCs seeded on the untreated and plasma-treated nanofibers for 1 and 3 min, appeared to be spindle shaped, elongated and healthier when compared to the poor and round- shaped cell morphology on the electrospun nanofibers treated with O_2 plasma for 5 and 10 min. Furthermore, the ADMSCs adopted randomized orientation owing to the randomly oriented nanofiber morphology. The enhanced cell adhesion and improved cell morphology on the O_2 plasma-treated electrospun nanofibers may be attributed to the presence of oxygen-containing polar functional groups on the surface of the nanofiber, which induces better interaction between the nanofibers and the cell surface integrin proteins. However, lower live cell density and poor cell morphology on the electrospun nanofibers treated with O_2 plasma for 5 and 10 min may be due to the free radicals present on the surface of the nanofibers, which induce unfavorable electrostatic interaction/oxidative stress causing cell death.

The live/dead staining results also demonstrate the cytocompatibility of the O_2 plasma- treated electrospun meshes matching the findings of the hemolysis and MTS results. It further reveals that O_2 plasma treatment for shorter period (1 and 3 min) aids favorable surface hydrophilicity towards cell adhesion and spreading when compared to those plasma-treated nanofibers for longer period (5 and 10 min).

Cytoskeletal architecture assessment

To further confirm the cell adhesion and cell morphology as observed during live/dead staining, the ADMSCs seeded on different electrospun nanofibers were stained using rhodamine conjugated to phalloidin after 72 h of culture, which again counter-stained with hochest for nucleus. Representative fluorescent images of ADMSCs seeded on different nanofibers are shown in Fig. 6e. The results confirm the ADMSCs attachment onto various electrospun nanofibers. The cell numbers counted from hochest nucleus staining were found to be 29 ± 4 (untreated), 33 ± 5 (1 min), 28 ± 5 (3 min), 26 ± 9 (5 min), and 18 ± 13 (10 min), while for TCP it is 78 ± 15 per image. Although, these numbers are not statistically different, it validated that there is no negative impact of O_2 plasma treatment for shorter period on the cell adhesion. It further validated our previous observation during hemolysis assay, MTS assay and live/dead staining that the plasma treatment for longer period (particularly, 5 and 10 min) do not hold biological efficiency in terms of hemocompatibility and cell growth. It is important to note that although TCP showed highest cell numbers attached to it, cell morphology is different from those on the electrospun nanofibers offering 3D paradigm for cell growth/spreading (polygonal shaped), while TCP is a flat surface (spindle shaped). Moreover, the cells grown on the untreated and O_2 plasma-treated electrospun nanofibers for 1, 3 and 5 min appeared to be bigger in size, when compared to that on the TCP. In fact, the ADMSCs grown on the TCP appeared to acquire a fibroblastic phenotype, characterized by wide spreading of cells (Ma et al. 2016). The randomized orientation of actin filaments of the ADMSCs grown on various electrospun nanofibers suggest cell spreading in random directions owing to the randomized nanofiber network.

Conclusion

In this study, the effect of treatment time of atmospheric pressure DBD O_2 plasma on the surface properties of silk/AMOX/PVA nanofibers is reported. The treatment time does not cause any morphological changes of the nanofibers which is confirmed by FESEM images. The plasma treatment time of 1–3 min facilitates incorporation of polar functional groups on the surface of the silk/AMOX/PVA nanofiber, which results in improved wettability and higher surface energy values. However, WVTR is observed to be reduced and comes within the suitable range for practical applications with increasing treatment time up to 1–3 min which further saturates with longer treatment time. Similarly, the plasma treatment for an appropriate time (1–3 min) also increases the tensile strength and Young's modulus of silk/AMOX/PVA nanofibers significantly. An increase in drug release rate is also observed with increase in treatment time which eventually helps in the antibacterial activity of the nanofibers for showing a good inhibition zone for a prolonged time. However, despite all the changes, the nanofibers do not show hemolytic effect independent of plasma treatment time. It is also evidenced that, silk/AMOX/PVA nanofibers plasma-treated for shorter period of time (1–3 min) not only shows improved cell viability (> 80%) but also promotes cell spreading with better cell adhesion. However, the rate of surface modification in every characterizations including wettability, surface energy, WVTR, tensile strength, Young's modulus, cell viability etc., are found highest for 1 min of O_2 plasma treatment. Therefore, all these findings can suggest that, DBD plasma treatment for shorter period

of time is sufficient for incorporating all the necessary surface modifications to the silk/AMOX/PVA nanofibers which embraces suitable wettability and WVTR, tensile strength and good cellular growth. Moreover, the mechanically stronger silk/AMOX/PVA/O_2 nanofibers can be used further for drug delivery applications where a faster release rate is required. The present study also provides the initial indication of future scope of using ADMSCs based approach in combination with the as-fabricated nanofibrous matrix with antibacterial properties in wound healing applications.

Acknowledgements This research work is supported by DST-SERB (Grant Nos. SR/FTP/PS-147/2012 and EMR/2016/006146) funded by the Department of Science and Technology (DST), India. Science and Technology (DST), Arup Jyoti Choudhury expresses his gratitude to the DST-INSPIRE Faculty Fellowship (Grant No. IFA14-PH-93) for the financial support to carry out this research work and Tezpur University, Assam, India for hosting the fellowship. Namita Ojah acknowledges the support provided by DST-INSPIRE and DST-SERB in the form of fellowship. The assistance of Kaushik Nath, Aftab Ansari, Dr. Dambarudhar Mohanta and Piyush Kumar Mishra, Department of Physics, Tezpur University, in carrying out the hemolysis test and UV measurement is acknowledged gratefully. The assistance of Dr. Saurav Haloi, Department of Molecular Biology and Biotechnology is acknowledged thankfully in carrying out the antibacterial tests.

Compliance with ethical standards

Conflict of interest The authors declare no conflict of interest.

Ethical approval This article does not contain any studies with human participants or animals performed by any of the authors.

References

Bae SH, Che JH, Seo JM, Jeong J, Kim ET, Lee SW, Koo KI, Suaning GJ, Lovell NH, Cho DD, Kim SJ, Chung H (2012) In vitro biocompatibility of various polymer-based microelectrode arrays for retinal prosthesis. Invest Ophthal Vis Sci 53:2653–2657

Balcon N, Aanesland A, Boswell R (2007) Pulsed RF discharges, glow and filamentary mode at atmospheric pressure in argon. Plas Sour Sci Technol 16:217–225

Baltazar-y-Jimenez A, Bistritz M, Schulz E, Bismarck A (2008) Atmospheric air pressure plasma treatment of lignocellulosic fibres: impact on mechanical properties and adhesion to cellulose acetate butyrate. Compo Sci Tech 68:215–227

Cestari M, Muller V, Rodrigues JHDS, Nakamura CV, Rubira AF, Muniz EC (2014) Preparing silk fibroin nanofibers through electrospinning: further heparin immobilization toward hemocompatibility improvement. Biomacromol 15:1762–1767

Choudhury AJ, Gogoi D, Kandimalla R, Kalita S, Choudhary YB, Khan MR, Kotoky J, Chutia J (2016) Penicillin impregnation on oxygen plasma surface functionalized chitosan/Antheraea assama silk fibroin: studies of antibacterial activity and antithrombogenic property. Mater Sci Engg C 60:475–484

Chouhan D, Mandal BB (2020) Silk biomaterials in wound healing and skin regeneration therapeutics: from bench to bedside. Acta Biomater 103:24–51

Chutia H, Kalita D, Mahanta C, Ojah N, Choudhury AJ (2019) Kinetics of inactivation of peroxidase and polyphenol oxidase intender coconut water by dielectric barrier discharge plasma. LWT-Food Sci Tech 101:625–629

Das P, Ojah N, Kandimalla R, Mohan K, Gogoi D, Duloi SK, Choudhury AJ (2018) Surface modification of electrospun PVA/chitosan nanofibers by dielectric barrier discharge plasma at atmospheric pressure and studies of their mechanical properties and biocompatibility. Int J Biol Macromol 114:1026–1032

Demirci S, Doğan A, Sahin F (2018) Role of adipose-derived stem cells in wound healing: an update from isolation to transplantation. Wound healing: stem cells repair and restorations, basic and clinical aspects, pp 133–147

Dyakonov T, Yang CH, Bush D, Gosangari S, Majuru S, Fatmi S (2012) Design and characterization of a silk-fibroin-based drug delivery platform using Naproxen as a model drug. J Drug Delivery 2012:490514

Foruzan E, Akmal AAS, Niayesh K, Lin J, Sharma DD (2018) Comparative study on various dielectric barriers and their effect on breakdown voltage. High Volt 3:51–59

Gomide VS, Zonari A, Ocarino NM, Goes AM, Serakides R, Pereira MM (2012) In vitro and in vivo osteogenic potential of bioactive glass–PVA hybrid scaffolds colonized by mesenchymal stem cells. Biomed Mater 7:01500

Hassan WU, Greiser U, Wang W (2014) Role of adipose-derived stem cells in wound healing. Wound Repair Regener 22:313–325

Hetemi D, Pinson J (2017) Surface functionalisation of polymers. Chem Soc Rev 46:5701

Jeong S, Yeo IS, Kim HN, Yoon YI, Jung SY, Min BM, Park WH (2009) Plasma-treated silk fibroin nanofibers for skin regeneration. Int J Biol Macromol 44:222–228

Kajdic S, Planinsek O, Gasperlin M, Kocbek P (2019) Electrospun nanofibers for customized drug-delivery systems. J Drug Delivery Sci Technol 51:672–681

Krishnakumar GS, Sampath S, Muthusamy S, John MA (2019) Importance of crosslinking strategies in designing smart biomaterials for bone tissue engineering: a systematic review. Mater Sci Engg C96:941–954

Kumar A, Borah R (2016) Effect of plasma irradiation on biocompatibility and cell adhesion of polyaniline/chitosan nanocomposites towards Hep G2 and PBMC cells. Adv Mater Proc 1:146–155

Kundu B, Kurland NE, Yadavalli VK, Kundu SC (2014) Isolation and processing of silk proteins for biomedical applications. Int J Bio Macromol 70:70–77

Lee M, Ko YG, Lee JB, Park WH, Cho D, Kwon OH (2014) Hydrophobization of silk fibroin nanofibrous membranes by fluorocarbon plasma treatment to modulate cell adhesion and proliferation behavior. Macromol Res 22:746–752

Liu B, Song YW, Jin L, Wang ZJ, Pu DY, Lin SQ, Zhou C, You HJ, Ma Y, Li JM, Yang L, Sung KLP, Zhang YG (2015) Silk structure and degradation. Colloids Surf B 131:122–128

Ma S, Xie N, Li W, Yuan B, Shi Y, Wang Y (2014) Immunobiology of mesenchymal stem cells. Cell Death Differ 24:216–225

Meghdadi M, Atyabi SM, Pezeshki-Modaress M, Irani S, Noormohammadi Z, Zandi M (2019) Cold atmospheric plasma as a promising approach for gelatin immobilization on poly(ε-caprolactone) electrospun scaffolds. Prog Biomater 8:65–75

Molavi AM, Sadeghi-Avalshahr A, Nokhasteh S, Naderi-Meshkin H (2020) Enhanced biological properties of collagen/chitosan-coated poly(ε-caprolactone) scaffold by surface modification with GHK-Cu peptide and 58S bioglass. Prog Biomater 9:25–34

Nedela O, Slepicka P, Švorčík V (2017) Surface modification of polymer substrates for biomedical applications. Mater 10:1115

Nuno A, Ribeiro GA, Pereira T, Amorim I, Fragoso J, Lopes A, Farnandes J, Costa E, Santos Silva A, Rodrigues M, Santos JD, Mauricio AC, Luis AL (2014) Biocompatibility and hemocompatibility of polyvinyl alcohol hydrogel used for vascular grafting—In vitro and in vivo studies. J Biomed Mater Res Part A 102:4262–4275

Ojah N, Saikia D, Gogoi D, Baishya P, Ahmed GA, Ramteke A, Choudhury AJ (2019) Surface modification of core-shell silk/PVA nanofibers by oxygen dielectric barrier discharge plasma: studies of physico-chemical properties and drug release behavior. App Surf Sci 475:219–229

Ojah N, DekaJ HS, Kandimalla R, Gogoi D, Medhi T, Mandal M, Ahmed GA, Choudhury AJ (2019) Chitosan coated silk fibroin surface modified by atmospheric dielectric-barrier discharge (DBD) plasma: a mechanically robust drug release system. J Biomater Sci Polym Ed 30:1–16

Ozkan A, Dufour T, Silva T, Britun N, Snyders R, Bogaerts A, Reniers F (2016) The influence of power and frequency on the filamentary behaviorof a flowing DBD application to the splitting of CO2. Plasma Sources Sci Technol 25:025013

Petlin DG, Tverdokhlebov SI, Anissimov YG (2017) Plasma treatment as an efficient tool for controlled drug release from polymeric materials: a review. J Cont Rel 266:57–74

Pollini M, Paladini F (2020) Bioinspired materials for wound healing application: the potential of silk fibroin. Materials 13:3361

Queen D, Gaylor JDS, Evans JH, Courtney JM, Reid WH (1987) The preclinical evaluation of the water vapour transmission rate through burn wound dressings. Biomaterials 8:367–371

Ray D, Subramanyam C (2016) CO_2 decomposition in a packed DBD plasma reactor: influence of packaging materials. RSC Adv 6:39492

Rezaei F, Shokri B, Sharifian M (2016) Atmospheric-pressure DBD plasma-assisted surface modification of polymethyl methacrylate: a study on cell growth/proliferation and antibacterial properties. App Sur Sci 360:641–651

Ribeiro VP, Almeida LR, Martins AR, Pashkuleva I, Marques AP, Ribeiro AS, Silva CJ, Bonifacio G, Sousa RA, Reis RL, Oliveira AL (2016) Influence of different surface modification treatments on silk biotextiles for tissue engineering applications. J Biomed Mater Res B104:496–507

Saeed SM, Hamid Mirzadeh H, Zandi M, Barzin J (2017) Designing and fabrication of curcumin loaded PCL/PVA multi-layer nanofibrous electrospun structures as active wound dressing. Prog Biomater 6:39–48

Shababdoust A, Ehsan M, Shokrollahi P, Zandi M (2018) Fabrication of curcumin-loaded electrospun nanofiberous polyurethanes with anti-bacterial activity. Prog Biomat 7:23–33

Simor M, Creyghton Y, Wypkema A, Zemek J (2010) The influence of surface DBD plasma treatment on the adhesion of coatings to high-tech textiles. J Adhes Sci Tech 24:77–97

Subia B, Kundu SC (2012) Drug loading and release on tumor cells using silk fibroin–albumin nanoparticles as carriers. Nanotechnology 24:035103

Theapsak S, Watthanaphanit A, Rujiravanit R (2010) Preparation of chitosan-coated polyethylene packagingfilms by DBD plasma treatment. ACS App Mater Interf 4:2474–2482

TomehMhd A, Hadianamrei R, Zhao X (2019) Silk fibroin as a functional biomaterial for drug and gene delivery. Pharmaceutics 11:494

Ujang Z, Rashid AHA, Suboh SK, Halim AS, Lim CK (2014) Physical properties and biocompatibility of oligochitosan membrane film as wound dressing. J Appl Biomater Funct Mater 12:155–162

Wang Y, Kim HJ, Vunjak-Novakovic G, Kaplan DL (2006) Stem cell-based tissue engineering with silk biomaterials. Biomaterials 27:6064–6082

Wang C, Lai PC, Syu SH, Leu J (2011) Effects of CF4 plasma treatment on the moisture uptake, diffusion and WVTR of poly(ethylene terephthalate) flexible films. Sur Coat Tech 206:318–324

Wang C, Zhang G, Wang X (2012) Comparisons of discharge characteristics of a dielectric barrier discharge with electrode structures. Vacuum 86:960–964

Williams KL, Godke RA, Bondioli KR (2011) Isolation and culture of porcine adipose tissue-derived somatic stem cells. Methods Mol Biol 702:77–86

Xiaoping T, Rongde Lu, Hui L (2012) Electrical characteristics of dielectric-barrier discharges in atmospheric pressure air using a power-frequency voltage source. Plasma Sci Technol 14:723

Xu R, Xia H, He W, Li Z, Zhao J, Liu B, Wang Y, Lei Q, Kong Y, Bai Y, Yao Z, Yan R, Li H, Zhan R, Yang S, Luo G, Wu J (2016) Controlled water vapor transmission rate promotes wound-healing via wound re-epithelialization and contraction enhancement. Sci Rep 6:24596

Yoshida S, Hagiwara K, Hasebe T, Hotta A (2013) Surface modification of polymers by plasma treatments for the enhancement of biocompatibility and controlled drug release. Sur Coat Tech 233:99–107

Yucel T, Lovett ML, Kaplan DL (2014) Silk-based biomaterials for sustained drug delivery. J Cont Rel 190:381–397

Zhang Z, Zhao Z, Zheng Z, Liu S, Mao S, Li X, Chen Y, Mao Q, Wang L, Wang F, Wang X, Pan Z, Li G (2019) Functionalization of polyethylene terephthalate fabrics using nitrogen plasma and silk fibroin/chitosan microspheres. App Sur Sci 495:143481